JACS
JOURNAL OF THE AMERICAN CHEMICAL SOCIETY

Article

pubs.acs.org/JACS

Optimized DNA "Nanosuitcases" for Encapsulation and Conditional Release of siRNA

Katherine E. Bujold, John C. C. Hsu, and Hanadi F. Sleiman*

Department of Chemistry, McGill University, and Center for Self-Assembled Chemical Structures, 801 Sherbrooke Street West, Montréal, Québec, Canada H3A 0B8

Supporting Information

ABSTRACT: We set out to design, synthesize, and optimize a DNA-minimal cage capable of encapsulating oligonucleotide drugs to facilitate their delivery. Through rational design and optimization using in vitro assays, we have assembled the first DNA "nanosuitcase" that can encapsulate a siRNA construct and release it upon recognition of an oligonucleotide trigger. The latter may be a mRNA or a microRNA (miRNA) which offers potential for dual or synergistic therapy. This construct assembles in near 100% yield, releases its cargo on demand, and can sustain biological conditions. Moreover, we find that the DNA scaffold is able to protect its cargo against site-specific cleavage and nuclease degradation. Release of the cargo is performed with fixed cells using a FRET-enabled construct imaged by confocal microscopy and reveals that the DNA cage remains responsive at the molecular level in a complex cellular environment. We foresee this construct will be able to address challenges in drug delivery, more specifically in nontoxic delivery and targeted release.

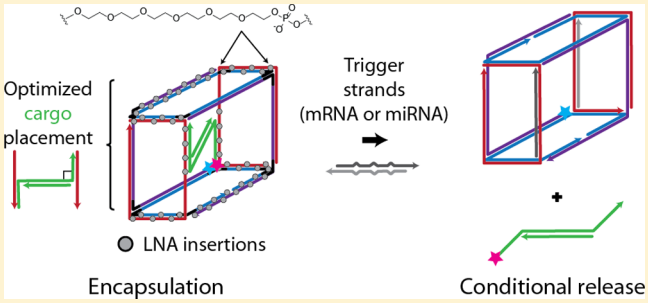

INTRODUCTION

DNA has found widespread use as a material in the field of structural DNA nanotechnology. Its predictable Watson–Crick base-pairing has been harnessed to create DNA-based nanomaterials with unmatched precision in two or three dimensions. Three main approaches exist that exploit different properties of DNA: (1) DNA tile assembly, which builds on DNA's rigidity to create designer tiles that form well-defined long-range assemblies,[1−5] (2) DNA origami, which utilizes a long strand of viral DNA as a backbone and folds it onto itself using staple strands, to create objects of any size and shape,[6−12] and (3) supramolecular DNA assembly which builds upon DNA's properties by incorporating synthetic insertions to access orthogonal modes of assembly.[13,14] We are interested in the latter approach, because it utilizes a DNA-minimal approach to create highly functional objects, which include DNA cages[15,16] and nanotubes[17,18] that can encapsulate hydrophobic micelles for drug delivery applications,[19] are functionalized with block copolymers,[20] gold nanoparticles,[21] quantum dots,[22] and sequence-specific polymers.[23] These polymer–DNA structures can in turn mediate the formation of higher-order assemblies,[24] increase resistance to nucleases,[25,26] and modulate cellular uptake.[27−32]

This ready access to DNA nanostructures of all shapes and sizes with functionalization and encapsulation capability, combined with their ready uptake by cells[33] represents an unparalleled opportunity to interface them with biology.[34−38] Numerous examples of DNA nanostructures have been reported that can elicit a specific biological response in vitro, in cells, or even in animal models.[39] More specifically, small and well-defined DNA cages have been used to deliver oligonucleotide drugs such as antisense oligonucleotides (AON),[40,41] CpG motifs,[42] proteins,[43] biopolymers,[44] and siRNAs.[39] Delivery of small molecules has also been achieved using doxorubicin intercalation in an origami[45−47] or a prismatic scaffold.[48] DNA cages were also found to be able to act as potential vaccines.[49] Yet, it remains challenging to precisely target these DNA cages to a cell type of interest since a significant portion of this observed uptake is nonspecific.[39,42,50,51]

A growing interest in targeted therapies has enabled the development of DNA nanostructures that will conditionally release their cargo upon recognition of a chosen target, allowing them to discriminate between healthy and cancerous cells, for example. Douglas et al. assembled an origami nanorobot that can encapsulate and selectively release its cargo upon recognition of a cell surface receptor.[8] DNA cages have also been functionalized with aptamers (short single-stranded oligonucleotides that bind with high affinity to a target), which allows them to discriminate between cell types.[48,50,52] Temperature has also been used as a trigger for the release of a protein encapsulated within a DNA nanocage.[43] Efforts toward this end have also been made using small conditional RNAs that perform shape and sequence transduction in the presence of a mRNA trigger of interest.[53] However, no DNA nanostructures exist that can conditionally deliver small

Received: August 10, 2016
Published: October 4, 2016

DOI: 10.1021/jacs.6b08369
J. Am. Chem. Soc. 2016, 138, 14030−14038

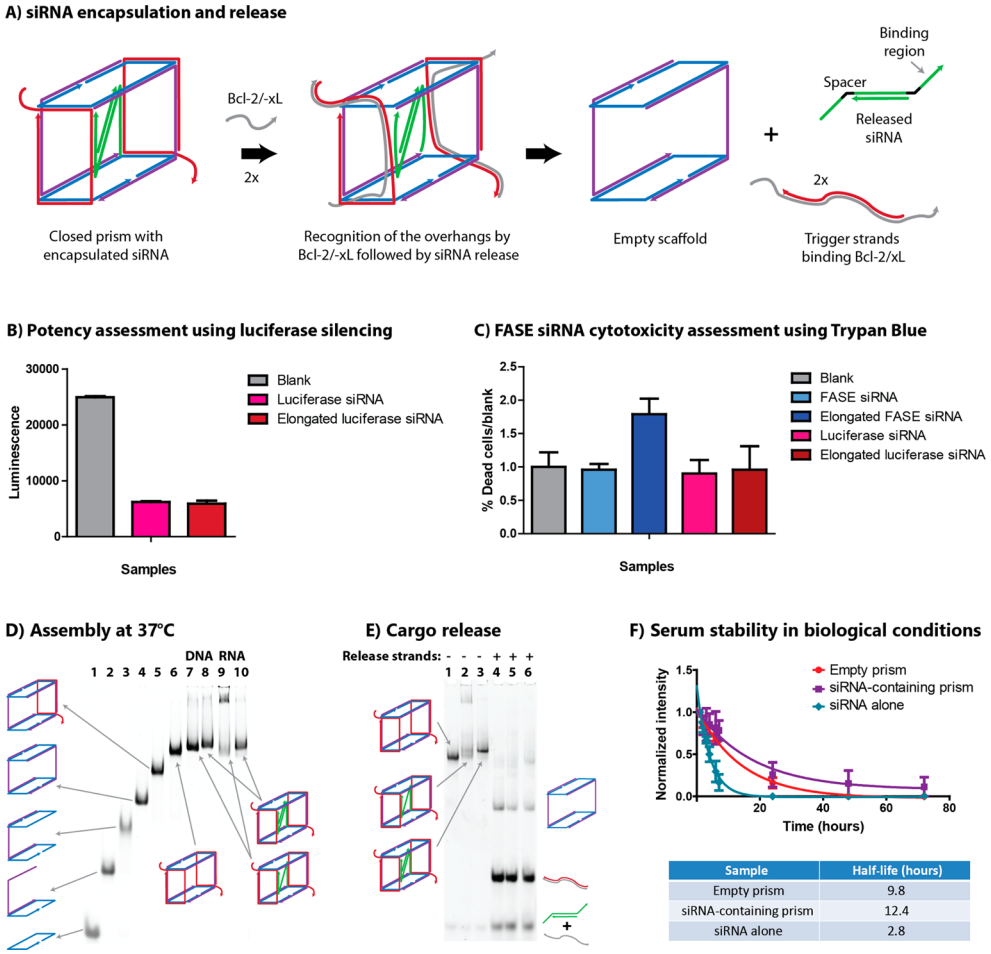

Figure 1. First design, potency, and properties of the siRNA-encapsulating prism. (A) Scheme showcasing the assembly of the prism and the siRNA release mechanism. The single-stranded overhangs (red strands) of the prism recognize and bind the Bcl-2 and/or Bcl-xL mRNA. Release of the encapsulated siRNA (green strands) occurs by strand displacement, yielding the empty scaffold, the siRNA which can elicit its effect in cells and the red trigger strands bound the Bcl-2/-xL mRNA which can act as antisense oligonucleotides. (B) Confirmation of the potency of the elongated luciferase siRNA. Both the classical and the elongated siRNA constructs reliably silence luciferase expression. (C) Assessment of the cytotoxicity of the FASE elongated siRNA using the Trypan blue dye exclusion assay. Compared to all controls, the elongated FASE siRNA causes more cell death after 72 h of incubation with LNCaP cells. (D) Stepwise assembly of the prism with single- (lane 7) and double-stranded DNA (lane 8, 90% yield) or single- (lane 9) and double-stranded siRNA (lane 10, 94% yield) cargo. (E) Release of the single- and double-stranded siRNA cargo from the prism. The prism (lane 1) with single- (lane 2) or double-stranded (lane 3) RNA cargo is incubated with cargo release strands. In all cases, the trigger strands recognize their complements and displace the gating strands (red), thus forming the empty scaffold (lanes 4–6) and releasing the cargo (lanes 5, 6). (F) Serum stability of the siRNA-containing prism in biological conditions. The siRNA encapsulated within the prism has a measured half-life of 12.4 h which is 4× superior to that of the siRNA alone.

molecule or oligonucleotide drugs based on cytoplasmic genetic markers. This approach would further direct the therapeutic effect of a given drug to a cell population of interest while preserving the drug until target recognition. It would also enable the design of "logic gates", or DNA molecules that release their drug cargo in response to a more complex population of different genetic markers.

Oligonucleotide drugs present a great deal of potential for gene therapy due to their potent and directed silencing of a gene of interest. Yet, their limited stability to nuclease degradation forces their packaging in liposomal or polymeric delivery vehicles that are often toxic, or necessitate the addition of multiple synthetic modifications which can be costly and time-consuming. It would be possible to design a DNA origami structure that releases siRNA drugs. However, these structures are composed of hundreds of DNA strands which complicates in vivo work. As an alternative, we propose to investigate DNA-minimal cages as well-defined transporters of oligonucleotide drugs and their potential for conditional drug delivery. More specifically, our aim is to identify the minimum number of DNA components that are required to achieve this functionality.

In this Article, we focus on the design and optimization of a trigger-responsive siRNA-encapsulating DNA cage in view of potential cellular applications. Building on findings from systematic iterations of design optimization and in vitro assays, we have assembled a DNA-minimal cage that can selectively encapsulate and protect a siRNA drug, and release it based on sequence recognition. This design can be engineered to respond to genetic markers present in the cell of interest or can readily be made to act as a dual therapeutic, if gated with antisense oligonucleotides or miRNAs. Overall, this approach opens the door to dual targeting or synergistic therapies with DNA cages.

DOI: 10.1021/jacs.6b08369
J. Am. Chem. Soc. 2016, 138, 14030–14038

RESULTS AND DISCUSSION

DNA Nanoswitch and siRNA Design. We hypothesized that encapsulating a siRNA within a DNA scaffold would confer significant stability and protection to the drug while offering potential for targeted delivery. For this purpose, we designed a DNA scaffold which can protect and selectively release a siRNA using two gates that recognize a chosen genetic marker (Figure 1A and Supporting Information section 3). Upon recognition of the marker, the two gating strands (Figure 1A, red strands; Supporting Information Scheme 1C) unwind by strand displacement,[54] thus liberating an encapsulated siRNA that is bound across the cavity (Figure 1A, green strands). Target recognition is accomplished using single-stranded overhangs that are complementary to the sequence of interest. Successful target recognition and unwinding releases the siRNA which can elicit further biological action; leaving behind the gating strands hybridized to their target and the empty DNA scaffold. Furthermore, the gating strands can act as antisense oligonucleotides, thus offering potential for dual therapy or synergistic action of two oligonucleotide drugs (Figure 1A). Overall, this design decouples the two recognition events, gate-opening and gene silencing.

At first, we sought to validate the potency of the siRNA encapsulated within the scaffold. Typically, siRNAs are composed of a fully duplexed core RNA of 21−24 bases flanked with 3′ overhangs that are 2 nucleotides in length.[55] Our design necessitates the siRNA to be elongated on both sides with DNA arms in order to hybridize to the scaffold. Short DNA spacers were also added on both sides of the siRNA to fit it within the cavity and improve flexibility (Figure 1A, Supporting Information Scheme 1B). Alterations to the length of the overhangs on the guide strand can affect the duration of gene silencing in vivo.[56] Accordingly, we chose to elongate the passenger strand on both sides, thus yielding a DNA-RNA chimera which can hybridize to the guide strand and the DNA scaffold.

It has been demonstrated that double-stranded synthetic siRNAs either with or without overhangs can promote efficient silencing in HeLa cells.[57] This property has allowed the direct conjugation of targeting ligands on the overhangs of the siRNA without affecting its activity.[58] In this study, luciferase was chosen as a target to verify the potency of the elongated siRNA. Through luciferase knockdown assays in HeLa cells that stably express luciferase, we found that the addition of the DNA arms on the passenger strand did not alter the potency of the siRNA when compared to the classical form of the siRNA. On the contrary, it was found on several occasions to slightly outperform the published sequence (Figure 1B, Supporting Information section 4).

As a control and for further demonstration of the potency of this type of siRNA, an elongated siRNA targeting fatty acid synthase (FASE) was tested, which provided an opportunity to test this construct in another cell line. Fatty acid synthase is an overexpressed gene in the LNCaP human prostate cancer cell line. Its knockdown with a siRNA leads to apoptosis and cytotoxicity after 72 h.[59] At first, we measured the levels of FASE protein expression after exposure to our RNA constructs using Western blots. We found the elongated siRNA against FASE to be slightly less active than its unmodified counterpart (Supporting Information section 5 and Figure 1). However, after observing recurrent lower protein counts (an indication of cell death) for the samples exposed to the modified FASE siRNA, an evaluation of the cytotoxicity of the construct was carried using the Trypan blue dye exclusion assay (Supporting Information section 6) which revealed a 2-fold increase in cell death, consistent with the increased potency of the elongated siRNA (Figure 1C).

Encapsulation and Release of siRNA within the Prism. Assessment of the ability of the DNA prism to assemble in high yields was carried out using polyacrylamide gel electrophoresis (PAGE) at 4 °C (Supporting Information section 7 and Figure 2) and 37 °C (Figure 1D) where the stepwise formation of this construct was monitored. The full prism was cleanly formed (Figure 1D, lane 6) with no side products. It was capable of encapsulating a control DNA cargo (Figure 1D, lane 8, 90% yield) and the elongated FASE siRNA. (Figure 1D, lane 10, 94% yield) (Supporting Information Table 8) Interestingly, there was an evident improvement in assembly yield at 37 °C compared to 4 °C (70% yield) consistent with the breaking up of less stable secondary interactions at higher temperature (Figure 1D, Supporting Information section 7 and Figure 2). On the other hand, the prism containing a single-stranded RNA within its cavity was found to form a structure whose mobility is consistent with a prism dimer, as evidenced by the lower mobility band in lane 9 (Figure 1D). This was hypothesized to be due to the RNA adopting a secondary structure in its single-stranded form due to an 8-base self-complementary portion that prevented both of its DNA sides from binding across the cavity, and instead facilitated intermolecular binding of another scaffold (Supporting Information Figure 3). In the double-stranded form, however, the siRNA strand can be cleanly encapsulated within the prism.

The release of the siRNA is controlled by two trigger strands (Supporting Information Scheme 1C, red strands) which specifically recognize Bcl-2 and Bcl-xL, two closely related antiapoptotic genes. This recognition strategy was inspired from a bispecific antisense oligonucleotide, which can be used to recognize both of these mRNA sequences due to the similarity of their sequences.[60] This antisense oligonucleotide is a perfect complement to the Bcl-2 mRNA sequence, however since Bcl-2 and Bcl-xL have very similar sequences, it can also repress the expression of Bcl-xL. We used this strategy to our advantage, by having one of the trigger strands be a perfect complement to Bcl-2 and the other to Bcl-xL. This allowed to reduce the symmetry of the prism (i.e., to use different strand sequences for the front and back gates), which then reduces the number of potential misassembled structures arising from the competition for binding sites on either side of the prism. In the present case, the two red strands are unique (yet similar) and will each bind preferentially to one side of the prism while retaining the same sensitivity to the target. As can be seen in Figure 1E, lane 6, cargo release was successful, after exposing the prism to the Bcl-2 and Bcl-xL sequences at 37 °C (Figure 1E, Supporting Information section 7). The yield of this release was ∼99% by nondenaturing PAGE.

Prism Stability in Biological Conditions. After ascertaining the potency, assembly and triggered release capabilities of the prism design, an evaluation of its properties in biological conditions was performed. At first, the thermal denaturation properties of the nanostructure were measured. The empty scaffold was found to melt at 66 °C, while the scaffold containing its double-stranded cargo melted at 65 °C, revealing that the cargo strands did not significantly perturb the scaffold stability upon binding (Supporting Information Figure 6 and section 8).

DOI: 10.1021/jacs.6b08369
J. Am. Chem. Soc. 2016, 138, 14030−14038

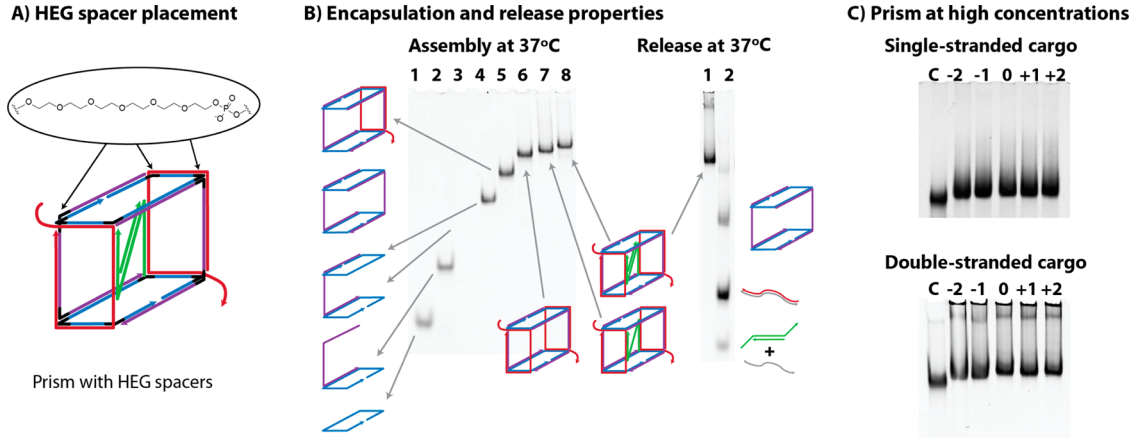

Figure 2. HEG spacer placement and impact on assembly and responsiveness. (A) Scheme outlining the placement of the 12 hexaethylene glycol spacers on the prism. (B) Addition of the HEG spacers does not impact the encapsulation and release properties of the prism at low concentrations which are both quantitative. (C) At high concentrations, the HEG spacers allow the encapsulation of a single-stranded cargo strand with no evidence of aggregation, independently of the length of the cargo strand (on the gel, expected length ± 2 bases). However, the addition of the complement to the cargo strand produces significant aggregation for every length tested, suggesting that the increased flexibility of the scaffold is not sufficient to guarantee the placement of the cargo inside the cavity.

Hahn and co-workers identified the physiological cation concentrations, more specifically the depletion of Mg^{2+}, and the digestion by nucleases present in fetal bovine serum (FBS) to be the two main challenges DNA nanostructures face as they are translated to the in vitro culture environment.[61] For this purpose, we measured the nuclease stability of the scaffold with its RNA cargo in the native state using 10% fetal bovine serum solutions in Dulbecco's modified Eagle medium (DMEM) utilizing the procedure developed by Conway et al. This procedure provides all the conditions DNA nanostructures encounter during cell assays: elevated temperatures, reduced magnesium concentrations and presence of nucleases.[25] We measured a half-life of 12 h for the siRNA encapsulated within the prism, which was in fact 4 times superior to the results obtained for the elongated siRNA construct alone. The structural integrity of the encapsulated siRNA was further verified over the course of the assay by denaturing the prism at different time points to ensure that it was not degraded by endonucleases. We found its onset of degradation to be between 10 and 24 h. This compared very favorably to unencapsulated siRNA alone which shows significant degradation after only 30 min (Figure 1F, Supporting Information Figure 8 and section 9). Taken together, these results demonstrate the enhanced ability of the prismatic scaffold to protect its cargo against nuclease degradation.

Introduction of Flexibility. One of the main strengths of this design is its ability to encapsulate a siRNA inside its cavity. However, if the size parameters of this cargo molecule are not exactly correct, it may become more favorable for the siRNA to bind intermolecularly to another scaffold instead of adopting the desired intramolecular binding pattern. We first noticed this type of behavior when concentrating the prism in view of cellular assays: a nonpenetrating band appeared on all PAGE controls (Supporting Information section 10 and Figure 9). This was further verified by dynamic light scattering (Supporting Information Figure 10 and Table 11). We attributed this behavior to the dynamic nature of this nanostructure. While at low concentrations, the encapsulated cargo remains inside the cavity, at higher concentrations, it has a higher propensity to adopt an intermolecular, cross-linked mode of binding which yields higher concentrations of dimers and undefined oligomeric or aggregated material.

In order to address these issues, we alleviated the strain experienced by the scaffold upon binding the cargo strands by inserting hexaethylene glycol (HEG) units on the corners of the scaffold (with the exception of the gating strands) since they display higher conformational freedom than DNA bases (Figure 2A, Supporting Information Scheme 1A). It was found using PAGE that the prism retained its clean assembly and selective release capabilities (Figure 2B).

The introduction of the HEG spacers, with their added flexibility, left some uncertainty as to the actual size of the cavity of the scaffold. To this effect, cargo strands of the estimated length ± 2 bases were synthesized and evaluated for their ability to bind the scaffold in the single- and double-stranded form. We found by PAGE that all five lengths were easily accommodated in the single-stranded form with no observable strain (Figure 2C). Some of them also yielded a small increase in melting temperature, consistent with increased stability (Supporting Information section 11, Figure 11, and Table 13). However, when in their double-stranded form, the cargo strands were found to produce significant aggregation by PAGE, suggesting that some strain remained (Figure 2C, Supporting Information section 11). Even though the HEG spacers did not completely solve this problem, we retained them in our design iterations since we believe that they will lend additional nuclease stability for future applications.[25] We also find that the addition of the HEG spacers provides extra breathing ability to the DNA nanostructure which is useful if one has to fit a cargo with a fixed length or when there is uncertainty as to the size of the cavity.

Optimization of Cargo Strand Orientation. Although the introduction of HEG spacers relieved the some of the strain experienced by the scaffold upon binding of the cargo strands, the remaining aggregation suggested another factor was at play. Further study of the scaffold and its cargo strands revealed the two acute angles the cargo strand had to adopt in order to bind the full length of the scaffold on both sides (Figure 3A). This binding mode is probably too strained for DNA which is an inherently rigid molecule and would explain the remaining aggregation behavior observed above. To counteract this effect,

DOI: 10.1021/jacs.6b08369
J. Am. Chem. Soc. 2016, 138, 14030−14038

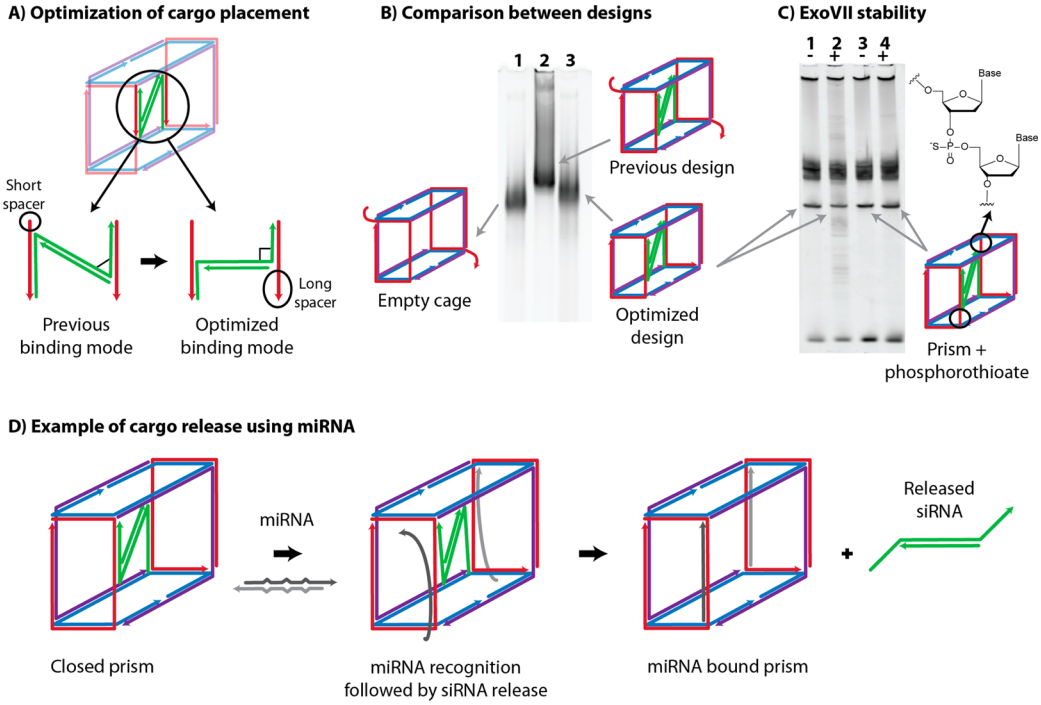

Figure 3. Redesign of the prism with optimized of cargo placement. (A) Schematic illustrating the modified angle that the cargo strands adopt upon binding the scaffold. This results in an increased spacer region which can be used as a trigger for cargo release. (B) Comparison between the previous design with HEG spacers (lane 2) and the new design with HEG spacers and an optimized cargo placement (lane 3). The new design now assembles as a single species even at elevated concentrations. (C) The new single-stranded regions are sensitive to ExoVII degradation (specific to single-stranded DNA) resulting in degradation of the scaffold and its cargo (lane 2 which is exposed to ExoVII shows more degradation products than the negative control in lane 1). Using a phosphorothioate backbone in those areas produces a prism that is resistant to ExoVII (lanes 3 and 4). (D) Example of a cargo release mechanism which releases a siRNA upon recognition of a miRNA sequence.

we increased the angle the cargo strand had to adopt by reducing the number of bases with which it hybridizes to the scaffold (Figure 3A, Supporting Information Scheme 1).

This modification left a single-stranded region next to the cargo strand that can be conveniently used as a trigger for target recognition and unwinding (Figure 3A and D, Supporting Information Scheme 1). It thus allowed the elimination of the single-stranded overhangs which tend to be sensitive to degradation.[27] As a result, only 21 bases of complementarity between the cargo and the DNA cages are now required to release the cargo, which is the length of one side of the prism. This allows the use of much shorter and biologically relevant triggers for release such as microRNAs (miRNAs). Fully processed miRNAs are 21−23 bases in length and have been identified as very promising cancer targets since they can affect the expression of many genes at once. Unique miRNA expression patterns have already been identified in cancer cells and can be acted upon by the addition of more miRNAs or antagomiRs which bind their complementary miRNAs and silence them.[62,63]

Assembly of this modified construct at 37 °C was successful with 85% yield (Supporting Information Figure 4A, lane 8), and no other side product than a dimer structure. For the first time, no evidence of aggregation was found upon concentrating this nanostructure up to 25 uM and comparison with the previous design iteration by PAGE shows a clearly improved assembly. (Figure 3B) We believe that any dimer structure arises from the 10mer binding regions of the scaffold which tend to be labile at this temperature (see below). The nanostructure also remains responsive to triggered release, and it releases the cargo in the presence of the Bcl-2/xL trigger strands (Supporting Information Figure 4B).

To evaluate the stability of these new single-stranded regions used for releasing the cargo as well as the dynamic character of the prism at 37 °C, we incubated the prism with Exonuclease VII, an enzyme which selectively degrades single-stranded DNA. In the present case, if the single-stranded regions are exposed or if the cage disassembles (thus producing single-stranded DNA regions), they will be degraded resulting in the release the cargo strand which will in turn be degraded. However, if the cargo remains bound to the scaffold, it will not be degraded since the enzyme does not degrade double-stranded DNA. We found the cargo was sensitive to this enzyme with approximately 50% being degraded under the assay's conditions (Figure 3C, lanes 1 and 2; Supporting Information Figure 12 and section 12). This suggested some instability of the scaffold to Exonuclease VII and we hypothesized that the single-stranded portions responsible for trigger recognition, as well as the single-stranded spacers on the trigger strand were probably being recognized and degraded as a consequence of the dynamic character of the 10mer and 11mer binding regions of the prism which provide a handle for the enzyme to start degrading the prism; ultimately weakening the cargo−scaffold interaction. We resynthesized these strands using a phosphorothioate backbone on the single-stranded portions. Replacing the endogenous phosphodiester backbone with phosphorothioate confers enhanced resistance to degradation by nucleases, but reduces binding affinity.[64] Thus, we only used these modifications in the single-stranded portions of our design. As expected, after this modification, the prism was

DOI: 10.1021/jacs.6b08369
J. Am. Chem. Soc. 2016, 138, 14030−14038

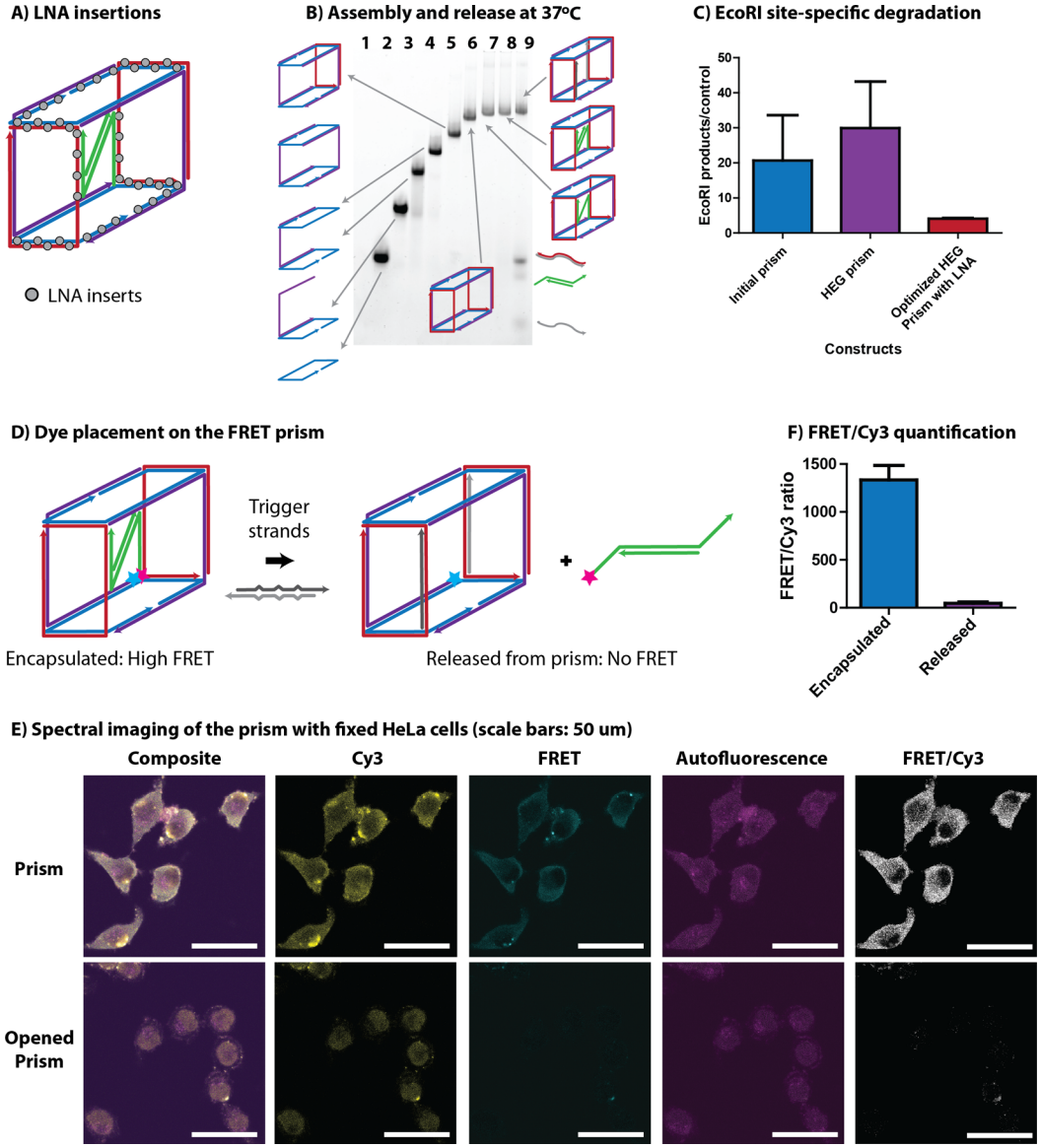

Figure 4. Design, assembly and properties of the LNA prism. (A) Scheme outlining the placement of the LNA inserts on the prism. (B) Quantitative assembly and release of the encapsulated cargo by PAGE. (C) Cargo protection against targeted degradation assay where the amount of *Eco*RI byproducts is measured versus a negative control not exposed to the enzyme. The prism with the HEG spacers, optimized cargo placement and LNA performs better than the previous design iteration since little to no *Eco*RI byproducts are detected. (D) Placement of the Cy3 and Cy5 dyes on the prism and cargo. A strong FRET signal is observed only when the cargo is encapsulated within the scaffold. Release of the cargo removes the FRET signal. (E) Sample images obtained from spectral imaging of the prism incubated with fixed cells before and after cargo release. The structural integrity of the prism is confirmed from the FRET signal. As expected, incubation with the release strands results in the loss of the FRET signal. (F) Quantification of the FRET/Cy3 ratio from spectral imaging for the FRET prism before and after cargo release.

found to be resistant to Exonuclease VII (Figure 3C, lanes 3 and 4; Supporting Information Figure 12).

Locked Nucleic Acids (LNA) Inserts. The current right-angled placement of the cargo strand on the scaffold increases the propensity for intramolecular binding and decreases dimer formation upon concentration of the prism. However, reducing the number of bases with which the cargo strands hybridize to the scaffold resulted in broader melting transitions and a loss in cooperativity upon melting (Supporting Information Figure 7 and Table 9). To address this observation, we inserted locked nucleic acids (LNA) monomers (approximately one every 3 bases) on the temperature-sensitive regions of the prism (Figure 4A, Supporting Information section 3). Each LNA monomer addition increases the melting temperature of a duplex by 2−8 °C.[65] While these insertions did not impact the assembly of the prism (Figure 4B, lane 8, 98% yield), we observed a clear increase in cooperativity upon melting compared to the previous design (Supporting Information Figure 7 and Table 9). Moreover, the prism melted at 63 °C in phosphate-buffered saline (PBS) (Supporting Information Figure 7 and section 8) which compares advantageously to the results in Figure 1, obtained in a magnesium buffer, known to stabilize DNA. Typically, a destabilization of 5−10 °C is observed when switching from a magnesium buffer to PBS and DNA origami structures are known to typically dissociate in nonmagnesium buffers.[61] More interestingly, our DNA-minimal prism with LNA inserts did not start to transition into single-stranded form before 40 °C which shows that it

DOI: 10.1021/jacs.6b08369
J. Am. Chem. Soc. 2016, 138, 14030−14038

easily maintains its conformation in reduced salt and elevated temperature conditions when compared to the unmodified prism.

The prism with LNA insertions also retains its siRNA-encapsulating and releasing abilities (Supporting Information Figure 5, lane 8, 93% yield of assembly). For this design iteration, the release of the cargo (DNA or siRNA) was performed using short 21-base release strands with random sequences to mimic miRNAs, yielding a small variation in the pattern produced (Figure 4B and Supporting Information Figure 5). Indeed, with this modification, the target strands bind and remain on the scaffold instead of displacing two of its component strands, thus yielding a lower mobility band for the empty scaffold than what was observed previously (Figure 3D).

One of the main roles of our DNA scaffold is to protect the encapsulated siRNA until its prescribed delivery location. At this stage, the combined stability of the prism at 37 °C and the absence of aggregation allowed an evaluation of its ability to protect the cargo against targeted degradation. To this effect, a site-specific degradation assay was devised, using the *Eco*RI restriction enzyme: the *Eco*RI restriction site, DNA double-stranded GAATTC, was inserted in the middle of DNA-only cargo strands, and the extent to which it was cut by the enzyme was measured (Supporting Information section 13). We found that, compared to the previous design iterations, the prism with LNA inserts and right-angle bound cargo was best at protecting its cargo, with little to no degradation products observed (Figure 4C, Supporting Information Figure 13 and Table 14). These results highlighted the importance of the previous design stages in ensuring that the cargo strands are bound with a favorable conformation and that the whole cage is stable under the conditions of interest.

Cargo Release in Fixed Cells. After ensuring the proper assembly and stability of the DNA "nanosuitcase" in biological conditions, we set out to evaluate its responsiveness in a complex cellular environment. For this purpose, we designed a DNA cage that exhibits FRET when it is fully assembled and loses this signal upon release of the cargo (Figure 4D, Supporting Information section 14 and Figure 14). This was accomplished through the strategic placement of Cy3 and Cy5 dyes on the scaffold; only when the cargo is released does the FRET signal disappear (Figure 4D). This strategy allows to evaluate the structural integrity of the DNA cage at the molecular level using the FRET signal between the two dyes and guarantees the cargo placement within the scaffold. We found through PAGE and fluorescence measurements that the DNA prism assembled quantitatively with both dyes and that they could be used to monitor the release of the cargo strands; a 3-fold decrease in FRET signal and a 2.3-fold enhancement in Cy3 emission were observed upon release of the cargo (Supporting Information section 14 and Figure 15).

Evaluation of the responsiveness of the prism in a cellular environment was carried using spectral imaging on a confocal microscope. This technique allows to collect the entire fluorescence emission spectrum of a given sample which can then be unmixed into its different components using an algorithm.[66] We incubated the FRET-enabled prism (Supporting Information Figure 16) with fixed HeLa cells in order to evaluate its structural integrity and responsiveness in a complex environment while decoupling them from its cellular fate. For this experiment, we were interested in separating the signal arising from the Cy3 emission, FRET, and cell autofluorescence after exciting the sample with a 514 nm laser beam (Supporting Information section 15). We found that this technique successfully separated each of these signals and were able to detect a significant FRET signal for the prism after its incubation with the cells, which was consistent with its maintained structural integrity in biological media and cells (Figure 4E, Supplementary Figure 17). Interestingly, the prism could also release its cargo in a cellular environment after incubation with short 21-base release strands. This resulted in near-complete loss of the FRET signal observed for the prism, thus confirming its responsiveness at the molecular level, even in crowded and Mg^{2+}-depleted environments. Quantification of the FRET/Cy3 ratio, which highlights the difference in FRET between samples,[66] for these images revealed a 29-fold decrease in the FRET signal upon release of the cargo, further demonstrating the responsiveness of the construct in complex cellular environments. (Figure 4F, Supporting Information section 15). We expect these constructs can find applications as reporters in live cell assays, especially in the investigation of the cellular uptake mechanisms of DNA nanostructures and their fate after internalization.

■ CONCLUSIONS

We have achieved the design and assembly of the first siRNA-encapsulating DNA "nanosuitcase". Our results demonstrate that the final nanostructure can assemble as a discrete object, protect its cargo, and selectively release it in the presence of chosen trigger strands in buffer, biological media, and complex cellular environments. The design parameters required to encapsulate the siRNA optimally within the construct do not affect its potency as it has been shown to work robustly on two different targets. Instead, the addition of HEG spacers increases the flexibility of the construct and together with the LNA insertions, its robustness. We find that the interplay between the stability of the nanostructure and its propensity to adopt a single structure under conditions of interest are paramount to its performing a desired function. We believe this construct can find wide applicability, since the gating strands and the encapsulated siRNA are decoupled, thus acting as logic gates, and can be tailored to any biological system of interest. Overall, the methods and the design presented here provide an overview of the steps involved in functional DNA-minimal cage design, while providing an adaptable nanostructure for potential biological applications. Future work will be aimed at optimizing the localization of this construct inside cells using targeting ligands and testing its ability to release its cargo in live cells on demand.

■ ASSOCIATED CONTENT

Supporting Information

The Supporting Information is available free of charge on the ACS Publications website at DOI: 10.1021/jacs.6b08369.

Experimental details on DNA prism design and characterization (PDF)

■ AUTHOR INFORMATION

Corresponding Author

*hanadi.sleiman@mcgill.ca

Notes

The authors declare no competing financial interest.

DOI: 10.1021/jacs.6b08369
J. Am. Chem. Soc. 2016, 138, 14030−14038

■ ACKNOWLEDGMENTS

The authors would like to thank NSERC, CIHR, the Canada Research Chairs Program, FRQNT, CSACS, and Prostate Cancer Canada for funding. The authors would also like to thank Dr. Erika Wee from the Advanced BioImaging Facility (ABIF) at McGill University for her help with the confocal imaging.

■ REFERENCES

(1) Winfree, E.; Liu, F.; Wenzler, L. A.; Seeman, N. C. *Nature* **1998**, *394*, 539−544.
(2) Lin, C.; Liu, Y.; Rinker, S.; Yan, H. *ChemPhysChem* **2006**, *7*, 1641−1647.
(3) Seeman, N. C. *Annu. Rev. Biochem.* **2010**, *79*, 65−87.
(4) Mao, C.; LaBean, T. H.; Reif, J. H.; Seeman, N. C. *Nature* **2000**, *407*, 493−496.
(5) Yan, H.; Park, S. H.; Finkelstein, G.; Reif, J. H.; LaBean, T. H. *Science* **2003**, *301*, 1882−1884.
(6) Rothemund, P. W. K. *Nature* **2006**, *440*, 297−302.
(7) Andersen, E. S.; Dong, M.; Nielsen, M. M.; Jahn, K.; Subramani, R.; Mamdouh, W.; Golas, M. M.; Sander, B.; Stark, H.; Oliveira, C. L. P.; Pedersen, J. S.; Birkedal, V.; Besenbacher, F.; Gothelf, K. V.; Kjems, J. *Nature* **2009**, *459*, 73−76.
(8) Douglas, S. M.; Bachelet, I.; Church, G. M. *Science* **2012**, *335*, 831−834.
(9) Han, D.; Pal, S.; Nangreave, J.; Deng, Z.; Liu, Y.; Yan, H. *Science* **2011**, *332*, 342−346.
(10) Douglas, S. M.; Dietz, H.; Liedl, T.; Hogberg, B.; Graf, F.; Shih, W. M. *Nature* **2009**, *459*, 414−418.
(11) Maune, H. T.; Han, S.-p.; Barish, R. D.; Bockrath, M.; Goddard, W. A., III; Rothemund, P. W. K.; Winfree, E. *Nat. Nanotechnol.* **2010**, *5*, 61−66.
(12) Wei, B.; Dai, M.; Yin, P. *Nature* **2012**, *485*, 623−626.
(13) Aldaye, F. A.; Palmer, A. L.; Sleiman, H. F. *Science* **2008**, *321*, 1795−1799.
(14) McLaughlin, C. K.; Hamblin, G. D.; Sleiman, H. F. *Chem. Soc. Rev.* **2011**, *40*, 5647−5656.
(15) Aldaye, F. A.; Sleiman, H. F. *J. Am. Chem. Soc.* **2007**, *129*, 13376−13377.
(16) McLaughlin, C. K.; Hamblin, G. D.; Aldaye, F. A.; Yang, H.; Sleiman, H. F. *Chem. Commun.* **2011**, *47*, 8925−8927.
(17) Aldaye, F. A.; Lo, P. K.; Karam, P.; McLaughlin, C. K.; Cosa, G.; Sleiman, H. F. *Nat. Nanotechnol.* **2009**, *4*, 349−352.
(18) Hamblin, G. D.; Carneiro, K. M. M.; Fakhoury, J. F.; Bujold, K. E.; Sleiman, H. F. *J. Am. Chem. Soc.* **2012**, *134*, 2888−2891.
(19) Edwardson, T. G. W.; Carneiro, K. M. M.; McLaughlin, C. K.; Serpell, C. J.; Sleiman, H. F. *Nat. Chem.* **2013**, *5*, 868−875.
(20) Carneiro, K. M. M.; Hamblin, G. D.; Hanni, K. D.; Fakhoury, J.; Nayak, M. K.; Rizis, G.; McLaughlin, C. K.; Bazzi, H. S.; Sleiman, H. F. *Chemical Science* **2012**, *3*, 1980−1986.
(21) Lau, K. L.; Hamblin, G. D.; Sleiman, H. F. *Small* **2014**, *10*, 660−666.
(22) Hamblin, G. D.; Rahbani, J. F.; Sleiman, H. F. *Nat. Commun.* **2015**, *6*, 7065.
(23) Edwardson, T. G. W.; Carneiro, K. M. M.; Serpell, C. J.; Sleiman, H. F. *Angew. Chem., Int. Ed.* **2014**, *53*, 4567−4571.
(24) Serpell, C. J.; Edwardson, T. G. W.; Chidchob, P.; Carneiro, K. M. M.; Sleiman, H. F. *J. Am. Chem. Soc.* **2014**, *136*, 15767−15774.
(25) Conway, J. W.; McLaughlin, C. K.; Castor, K. J.; Sleiman, H. *Chem. Commun.* **2013**, *49*, 1172−1174.
(26) Keum, J.-W.; Bermudez, H. *Chem. Commun.* **2009**, 7036−7038.
(27) Bujold, K. E.; Fakhoury, J.; Edwardson, T. G. W.; Carneiro, K. M. M.; Briard, J. N.; Godin, A. G.; Amrein, L.; Hamblin, G. D.; Panasci, L. C.; Wiseman, P. W.; Sleiman, H. F. *Chemical Science* **2014**, *5*, 2449−2455.
(28) Rush, A. M.; Thompson, M. P.; Tatro, E. T.; Gianneschi, N. C. *ACS Nano* **2013**, *7*, 1379−1387.
(29) Wu, Y.; Sefah, K.; Liu, H.; Wang, R.; Tan, W. *Proc. Natl. Acad. Sci. U. S. A.* **2010**, *107*, 5−10.
(30) Chien, M.-P.; Rush, A. M.; Thompson, M. P.; Gianneschi, N. C. *Angew. Chem., Int. Ed.* **2010**, *49*, 5076−5080.
(31) Gissot, A.; Oumzil, K.; Patwa, A.; Barthelemy, P. *New J. Chem.* **2014**, *38*, 5129−5134.
(32) Liu, H.; Zhu, Z.; Kang, H.; Wu, Y.; Sefan, K.; Tan, W. *Chem. - Eur. J.* **2010**, *16*, 3791−3797.
(33) Walsh, A. S.; Yin, H.; Erben, C. M.; Wood, M. J. A.; Turberfield, A. J. *ACS Nano* **2011**, *5*, 5427−5432.
(34) Lo, P. K.; Metera, K. L.; Sleiman, H. F. *Curr. Opin. Chem. Biol.* **2010**, *14*, 597−607.
(35) Chao, J.; Liu, H.; Su, S.; Wang, L.; Huang, W.; Fan, C. *Small* **2014**, *10*, 4626−4635.
(36) Linko, V.; Ora, A.; Kostiainen, M. A. *Trends Biotechnol.* **2015**, *33*, 586−594.
(37) Chen, Y.-J.; Groves, B.; Muscat, R. A.; Seelig, G. *Nat. Nanotechnol.* **2015**, *10*, 748−760.
(38) Lanier, L. A.; Bermudez, H. *Curr. Opin. Chem. Eng.* **2015**, *7*, 93−100.
(39) Lee, H.; Lytton-Jean, A. K. R.; Chen, Y.; Love, K. T.; Park, A. I.; Karagiannis, E. D.; Sehgal, A.; Querbes, W.; Zurenko, C. S.; Jayaraman, M.; Peng, C. G.; Charisse, K.; Borodovsky, A.; Manoharan, M.; Donahoe, J. S.; Truelove, J.; Nahrendorf, M.; Langer, R.; Anderson, D. G. *Nat. Nanotechnol.* **2012**, *7*, 389−393.
(40) Fakhoury, J. J.; McLaughlin, C. K.; Edwardson, T. W.; Conway, J. W.; Sleiman, H. F. *Biomacromolecules* **2014**, *15*, 276−282.
(41) Keum, J.-W.; Ahn, J.-H.; Bermudez, H. *Small* **2011**, *7*, 3529−3535.
(42) Li, J.; Pei, H.; Zhu, B.; Liang, L.; Wei, M.; He, Y.; Chen, N.; Li, D.; Huang, Q.; Fan, C. *ACS Nano* **2011**, *5*, 8783−8789.
(43) Juul, S.; Iacovelli, F.; Falconi, M.; Kragh, S. L.; Christensen, B.; Frøhlich, R.; Franch, O.; Kristoffersen, E. L.; Stougaard, M.; Leong, K. W.; Ho, Y.-P.; Sørensen, E. S.; Birkedal, V.; Desideri, A.; Knudsen, B. R. *ACS Nano* **2013**, *7*, 9724−9734.
(44) Bhatia, D.; Surana, S.; Chakraborty, S.; Koushika, S. P.; Krishnan, Y. *Nat. Commun.* **2011**, *2*, 339.
(45) Jiang, Q.; Song, C.; Nangreave, J.; Liu, X.; Lin, L.; Qiu, D.; Wang, Z.-G.; Zou, G.; Liang, X.; Yan, H.; Ding, B. *J. Am. Chem. Soc.* **2012**, *134*, 13396−13403.
(46) Zhang, Q.; Jiang, Q.; Li, N.; Dai, L.; Liu, Q.; Song, L.; Wang, J.; Li, Y.; Tian, J.; Ding, B.; Du, Y. *ACS Nano* **2014**, *8*, 6633−6643.
(47) Ouyang, X.; Li, J.; Liu, H.; Zhao, B.; Yan, J.; Ma, Y.; Xiao, S.; Song, S.; Huang, Q.; Chao, J.; Fan, C. *Small* **2013**, *9*, 3082−3087.
(48) Chang, M.; Yang, C.-S.; Huang, D.-M. *ACS Nano* **2011**, *5*, 6156−6163.
(49) Liu, X.; Xu, Y.; Yu, T.; Clifford, C.; Liu, Y.; Yan, H.; Chang, Y. *Nano Lett.* **2012**, *12*, 4254−4259.
(50) Charoenphol, P.; Bermudez, H. *Mol. Pharmaceutics* **2014**, *11*, 1721−1725.
(51) Li, J.; Fan, C.; Pei, H.; Shi, J.; Huang, Q. *Adv. Mater.* **2013**, *25*, 4386−4396.
(52) Zhu, G.; Zheng, J.; Song, E.; Donovan, M.; Zhang, K.; Liu, C.; Tan, W. *Proc. Natl. Acad. Sci. U. S. A.* **2013**, *110*, 7998−8003.
(53) Hochrein, L. M.; Schwarzkopf, M.; Shahgholi, M.; Yin, P.; Pierce, N. A. *J. Am. Chem. Soc.* **2013**, *135*, 17322−17330.
(54) Zhang, D. Y.; Seelig, G. *Nat. Chem.* **2011**, *3*, 103−113.
(55) Deleavey, G. F.; Damha, M. J. *Chem. Biol.* **2012**, *19*, 937−954.
(56) Strapps, W. R.; Pickering, V.; Muiru, G. T.; Rice, J.; Orsborn, S.; Polisky, B. A.; Sachs, A.; Bartz, S. R. *Nucleic Acids Res.* **2010**, *38*, 4788−4797.
(57) Czauderna, F.; Fechtner, M.; Dames, S.; Aygün, H.; Klippel, A.; Pronk, G. J.; Giese, K.; Kaufmann, J. *Nucleic Acids Res.* **2003**, *31*, 2705−2716.
(58) Dua, P.; Kim, S.; Lee, D.-k. *Methods* **2011**, *54*, 215−225.
(59) De Schrijver, E.; Brusselmans, K.; Heyns, W.; Verhoeven, G.; Swinnen, J. V. *Cancer Res.* **2003**, *63*, 3799−3804.

DOI: 10.1021/jacs.6b08369
J. Am. Chem. Soc. 2016, 138, 14030−14038

(60) Yamanaka, K.; Rocchi, P.; Miyake, H.; Fazli, L.; So, A.; Zangemeister-Wittke, U. W. E.; Gleave, M. E. *BJU Int.* **2006**, *97*, 1300−1308.
(61) Hahn, J.; Wickham, S. F. J.; Shih, W. M.; Perrault, S. D. *ACS Nano* **2014**, *8*, 8765−8775.
(62) Stenvang, J.; Petri, A.; Lindow, M.; Obad, S.; Kauppinen, S. *Silence* **2012**, *3*, 1−1.
(63) Li, Z.; Rana, T. M. *Nat. Rev. Drug Discovery* **2014**, *13*, 622−638.
(64) Kibler-Herzog, L.; Zon, G.; Uznanski, B.; Whittier, G.; Wilson, W. D. *Nucleic Acids Res.* **1991**, *19*, 2979−2986.
(65) Koshkin, A. A.; Singh, S. K.; Nielsen, P.; Rajwanshi, V. K.; Kumar, R.; Meldgaard, M.; Olsen, C. E.; Wengel, J. *Tetrahedron* **1998**, *54*, 3607−3630.
(66) Broussard, J. A.; Rappaz, B.; Webb, D. J.; Brown, C. M. *Nat. Protoc.* **2013**, *8*, 265−281.

DOI: 10.1021/jacs.6b08369
J. Am. Chem. Soc. 2016, 138, 14030−14038